JOURNAL OF AIRCRAFT
Vol. 38, No. 1, January–February 2001

# Coupled Rotor/Fuselage Vibration Analysis for Teetering Rotor and Test Data Comparison

Hyeonsoo Yeo* and Inderjit Chopra†
*University of Maryland, College Park, Maryland 20742*

**A comprehensive vibration analysis of a coupled rotor/fuselage system for a two-bladed teetering rotor using finite element methods in space and time is developed that incorporates consistent rotor/fuselage structural, aerodynamic, and inertial couplings and a modern free-wake model. Coupled nonlinear periodic blade and fuselage equations are transformed to the modal space and solved simultaneously. The elastic line airframe model of the AH-1G helicopter is integrated into the elastic rotor finite element model. Analytical predictions of rotor control angles, blade loads, hub forces, and vibration are compared with AH-1G operation load survey test data. The blade loads predicted by the present analysis show generally fair agreement with the flight test data. Calculated 2 and 4 per revolution vertical vibration levels at the pilot seat show fair correlation with the flight test, but the predicted 2 per revolution lateral vibration level is higher than the measurement, particularly at high advance ratios. Modeling of pylon flexibility is essential in the two-bladed teetering rotor vibration analysis. Refined aerodynamics such as free wake and unsteady aerodynamics have an important role in the prediction of vibration.**

## Nomenclature

| | | |
|---|---|---|
| $e_g$ | = | blade center-of-gravity offset from the elastic axis |
| $l_u$ | = | undersling |
| $m$ | = | blade mass per unit length |
| $\boldsymbol{p}_{\mathrm{f_e}}$ | = | temporal fuselage elastic modal displacement vector |
| $\boldsymbol{p}_{\mathrm{f_r}}$ | = | temporal fuselage rigid modal displacement vector |
| $R$ | = | blade radius |
| $u, v, w$ | = | blade elastic displacements in the axial, lag, and flap directions |
| $x$ | = | longitudinal coordinate |
| $\dot{x}_f, \dot{y}_f, \dot{z}_f$ | = | fuselage translational velocities |
| $\ddot{x}_f, \ddot{y}_f, \ddot{z}_f$ | = | fuselage translational accelerations |
| $\dot{\alpha}_s, \dot{\phi}_s, \dot{\psi}_s$ | = | fuselage pitch, roll, and yaw rates |
| $\ddot{\alpha}_s, \ddot{\phi}_s, \ddot{\psi}_s$ | = | fuselage pitch, roll, and yaw accelerations |
| $\beta_p$ | = | precone angle |
| $\beta_T$ | = | teeter angle |
| $\eta_r$ | = | distance from blade elastic axis to blade three-quarter chord |
| $\theta_0$ | = | rigid pitch angle due to control pitch and pretwist |
| $\lambda$ | = | rotor inflow |
| $\mu$ | = | advance ratio |
| $\xi$ | = | temporal blade modal displacement vector |
| $\hat{\phi}$ | = | blade elastic twist |
| $\psi$ | = | rotor azimuth angle |
| $\Omega$ | = | rotational speed of rotor |

*Subscripts*

| | | |
|---|---|---|
| $r\mathrm{f_e}$ | = | rotor/fuselage elastic motion coupling terms |
| $r\mathrm{f_r}$ | = | rotor/fuselage rigid motion coupling terms |
| $rt$ | = | rotor/teetering motion coupling terms |

## Introduction

HELICOPTERS suffer from excessive vibration because of the unsteady aerodynamic environment at the rotor disk, nonlinear inertial couplings of slender rotating blades, and complex rotor-fuselage interactional effects. A high level of vibration can cause fatigue failure of components and human discomfort, thus seriously affecting ride quality and system reliability, increasing maintenance costs, and degrading equipment performance. Identification of vibration problems and the design of vibration reduction devices have been dependent on flight test data because of insufficient vibration prediction capability. Therefore, adequate accurate vibration prediction methodology is essential for the design of low-vibration helicopters with cost and time effectiveness.

During the last two decades, coupled rotor/fuselage vibration analyses have been developed by many researchers using a variety of assumptions and solution methods.[1] They all emphasized the importance of understanding the fully coupled aeroelastic rotor/fuselage system.

One way of accounting for the interactions between airframe vibratory motion and rotor vibratory loads is to calculate the rotor and the fuselage impedances separately and determine compatible vibratory hub loads by matching displacements and forces at the hub. The concept of impedance matching in a coupled rotor/airframe vibration analysis was first proposed by Gerstenberger and Wood.[2] By the use of the impedance matching method, simplified investigations such as those reported in Refs. 3–6, have made significant contributions to the understanding of the basic characteristics of rotorcraft vibration. A simple rotor/fuselage model and highly simplified aerodynamics were used to determine the vibration of a fuselage. The rotor blade was often assumed to undergo only flapping motion. For the calculation of airframe impedance, simple airframe models were used such as a rotor support system modeled as concentrated inertias and springs,[4] and a uniform beam model representing plunge, roll, and pitch motions.[5] It was shown that hub vibratory loads determined using a hub-fixed analysis were inadequate for the prediction of vibration.

Stephens and Peters[7] investigated an iteration method and a fully coupled method to predict vibration of a coupled rotor/body system. In the iteration method, rotor and body responses were calculated separately, and the coupling was achieved through the iteration process. In the fully coupled method, coupled rotor/body equations were solved simultaneously. It was shown that even though both methods are identical in terms of physical representation, convergence of the iteration approach is dependent on the coupling mass ratio. It was shown that the convergence is not guaranteed if the supporting system mass is less than the rotor mass.

Because the preceding analyses were based mostly on either simple rotor blade models or very idealized fuselage models, they

Received 8 April 1999; revision received 18 April 2000; accepted for publication 22 April 2000. 

*Graduate Research Assistant, Alfred Gessow Rotorcraft Center, Department of Aerospace Engineering; currently Research Scientist, Raytheon Technical Services Company, NASA Ames Research Center, Moffett Field, CA 94035. Member AIAA.

†Alfred Gessow Professor and Director, Alfred Gessow Rotorcraft Center, Department of Aerospace Engineering. Fellow AIAA.

yielded only qualitative trends. It is now well established that nonlinear blade forces contribute significantly to vibratory hub loads. Thus, a consistent set of nonlinear coupled rotor/fuselage equations of motion is essential in the prediction of vibration.

Recently, there have been focused studies to improve the modeling of a coupled rotor/fuselage system. Vellaichamy and Chopra[8] presented a coupled rotor/fuselage analysis using an elastic blade and flexible fuselage modeling (stick model). Each blade was modeled to be an elastic beam undergoing flap bending, lead/lag bending, elastic twist, and axial deflection. A finite element method in time was used to solve blade steady response, and a harmonic balance method was used to calculate body response due to periodic hub forcing. The rotor/body coupling was achieved using an iterative procedure. Chiu and Friedmann[9] developed a coupled rotor/flexible fuselage model for vibration reduction studies. A collection of elements (beam, truss, and plate) were used to model a three-dimensional fuselage. The coupled elastic blade flap/lag/torsion equations, elastic and rigid fuselage equations, and the overall vehicle trim equations were solved using a harmonic balance technique. However, these analyses incorporated highly idealized aerodynamics such as uniform or linear inflow and quasi-steady aerodynamics so that vibration was substantially underpredicted.

Helicopter vibration is due to the higher harmonic airloading of the rotor; thus, nonuniform induced velocities caused by blade vortices can be a key factor in the prediction of vibration. Therefore, refined aerodynamic models such as free wake and unsteady aerodynamics are essential in predicting rotor vibratory loads and fuselage vibration accurately. Hansford and Vorwald[10] compared predictions of vibratory blade and hub loads from several different comprehensive analyses with Lynx flight-test data and showed the need of refined aerodynamics models to predict vibratory loads accurately. For example, unless a free-wake model is incorporated in rotor analysis, predicted vibratory loads could be an order of magnitude lower than measured values for both low- and high-speed regimes.

NASA Langley Research Center carried out a successful design analysis methods for vibrations (DAMVIBS) program to establish the technology for accurate and reliable vibration prediction capability during the design of a rotorcraft. Four major helicopter manufacturers (Bell Helicopter Textron, The Boeing Company, former McDonnell Douglas Helicopter Company, and Sikorsky Aircraft) actively participated in this program. Systematic modeling and analysis techniques were investigated, including airframe finite element modeling, modeling refinements for difficult components, coupled rotor/airframe vibration analysis, and airframe structural optimization. They developed state-of-the-art finite element models for the airframe, conducted ground vibration tests, and made test/analysis comparisons. Under the DAMVIBS program, the four helicopter companies also applied their own methods to calculate the vibrations of the AH-1G helicopter and correlated the predictions with operational load survey (OLS) flight-test data.[11–14] They identified modeling requirements for the vibration analysis of complex helicopter structures and rotor/fuselage coupling effects. Most of the analyses were unable to predict vibration accurately for all flight conditions. These studies pointed out that the coupled rotor/fuselage vibration analysis should be improved to be useful for the design and development of a rotor/airframe system.

This paper develops a comprehensive vibration analysis of a coupled rotor/fuselage system for a two-bladed teetering rotor using finite element methods in space and time. Rotor/fuselage structural, aerodynamic, and inertial couplings are consistently derived and presented in explicit form. For the calculation of inflow and blade loads, a pseudoimplicit free-wake model[15] and time-domain unsteady aerodynamics[16] are incorporated. The effect of compressibility (Prandtl–Glauert correction) and reversed flow are also included in the aerodynamic model. The elastic line model of the AH-1G helicopter is integrated with the two-bladed teetering elastic rotor finite element model. Vibration levels are calculated at several different flight conditions and are compared with the flight-test data.

## Formulation and Solution Procedure

The baseline rotor analysis is taken from UMARC,[17] where each blade is assumed to be an elastic beam undergoing flap and lag bending, elastic twist, and axial deflection. The analysis for a two-bladed teetering rotor is formulated and incorporated into UMARC. A teetering rotor has two blades that are hinged at the rotational axis, that is, on the shaft, and usually uses no independent flap or lead/lag offset hinges. For steady dynamic analysis of conventional rotors with identical blades, it is usually sufficient to trace the motion of one blade only and then build motions of other blades using proper phase angles. In the analysis of the teetering rotor, however, it is necessary to treat two blades simultaneously because the two blades are rigidly connected to each other and attached to the mast through a common flapping hinge. The elastic rotor coupled equations include six hub degrees of motion. The airframe is discretized into beam elements, each undergoing vertical and lateral bending, elastic twist, and axial deformation. The rotor vibratory loads are transmitted to the fuselage through the hub, and the effects of fuselage motion are included in the determination of blade loads. The coupled rotor/fuselage formulation is described in detail in Ref. 18 and is summarized in this paper.

The derivation of the coupled rotor/fuselage equations of motion are based on Hamilton's variational principle generalized for a nonconservative system. It can be expressed as

$$\delta\Pi = \int_{t_1}^{t_2} (\delta U - \delta T - \delta W)\,\mathrm{d}t = 0 \tag{1}$$

where $\delta U$ is the virtual variation of strain energy, $\delta T$ is the virtual variation of kinetic energy, and $\delta W$ is the virtual work done by external forces. These virtual variations take into consideration contributions from both the rotor and the fuselage.

### Coordinate Systems

Coordinate systems to model a two-bladed teetering rotor are shown in Fig. 1. Usually a teetering rotor has the main rotor hub at a distance below a teetering axis. This design practice is called undersling and is adopted to reduce Coriolis forces induced by teetering motion. For odd harmonics of the flap moment that result in a net flap moment on the hub, the blade acts as an articulated rotor with no hinge offset. For even harmonics, where the flap moments are reacted internally in the hub, the blade acts as a hingeless rotor. To consider both the articulated and the hingeless rotor characteristics of a teetering rotor, first a teetering angle $\beta_T$ is introduced. Then on top of that, blade elastic deformation is defined. The coordinate transformation between the hub-fixed rotating system and the undeformed blade coordinate system is given by

$$\begin{Bmatrix} \hat{i} \\ \hat{j} \\ \hat{k} \end{Bmatrix} = \begin{bmatrix} \cos(\beta_p + \beta_T) & 0 & \sin(\beta_p + \beta_T) \\ 0 & 1 & 0 \\ -\sin(\beta_p + \beta_T) & 0 & \cos(\beta_p + \beta_T) \end{bmatrix} \begin{Bmatrix} \hat{I} \\ \hat{J} \\ \hat{K} \end{Bmatrix} \tag{2}$$

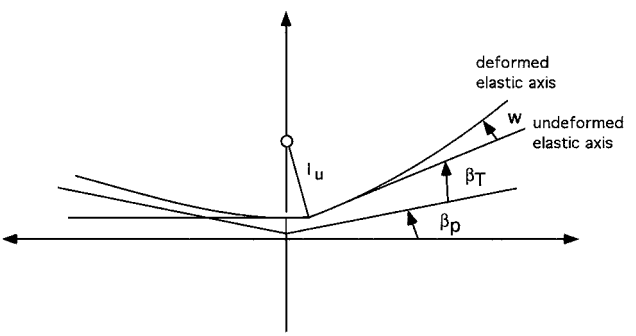


**Fig. 1 Coordinate system of a teetering rotor.**

where $\beta_p$ is a precone angle. The preceding transformation matrix is used to obtain blade velocities and accelerations for calculation of the aerodynamic loads and kinetic energy.

**Ordering Scheme**

During the derivation, an ordering scheme is used to simplify the equations of motion. Terms up second order are retained in the analysis by introducing a nondimensional quantity $\epsilon$, where $\epsilon$ is a quantity equivalent to the maximum bending rotation expected in the beam model, that is,

$$\mathcal{O}(1) + \mathcal{O}(\epsilon^2) \approx \mathcal{O}(1) \tag{3}$$

The order of important nondimensional quantities associated the formulation are listed as follows:

$$\mathcal{O}(1) = \mu, \cos\psi, \sin\psi, \cos\theta_0, \sin\theta_0, \frac{\partial}{\partial\psi} \tag{4}$$

$$\mathcal{O}(\epsilon) = v/R, w/R, \beta_p, \beta_T, l_u/R, \hat{\phi} \tag{5}$$

$$\mathcal{O}\left(\epsilon^{\frac{3}{2}}\right) = \dot{x}_F/\Omega R, \dot{y}_F/\Omega R, \dot{z}_F/\Omega R, \dot{\alpha}_s, \dot{\phi}_s, \dot{\psi}_s \tag{6}$$

**Kinetic Energy**

To derive the kinetic energy expression for the blade, we need the blade velocity in the deformed frame. This velocity consists of blade motion relative to the hub plus the motion of the hub itself. This relation is expressed as

$$\boldsymbol{V} = \boldsymbol{V}_b + \boldsymbol{V}_f \tag{7}$$

where $\boldsymbol{V}_b$ is the velocity of the blade relative to the hub and $\boldsymbol{V}_f$ is the velocity of the blade induced by the motion of the fuselage. The blade velocity is expressed in the deformed frame as follows:

$$\boldsymbol{V} = (V_{bx} + V_{fx})\hat{i} + (V_{by} + V_{fy})\hat{j} + (V_{bz} + V_{fz})\hat{k} \tag{8}$$

where

$$V_{bx} = \dot{x}_1 - y_1\cos(\beta_p + \beta_T) - (z_1 - l_u)\dot{\beta}_T \tag{9}$$

$$V_{fx} = (\dot{x}_F - h\dot{\alpha}_s - y_{cg}\dot{\psi}_s)\cos\psi + (\dot{y}_F + h\dot{\phi}_s + x_{cg}\dot{\psi}_s)\sin\psi \tag{10}$$

$$V_{by} = \dot{y}_1 + (x_1 - l_u\beta_p)\cos(\beta_p + \beta_T) - (z_1 - l_u)\sin(\beta_p + \beta_T) \tag{11}$$

$$V_{fy} = -(\dot{x}_F - h\dot{\alpha}_s - y_{cg}\dot{\psi}_s)\sin\psi + (\dot{y}_F + h\dot{\phi}_s + x_{cg}\dot{\psi}_s)\cos\psi + x\dot{\psi}_s \tag{12}$$

$$V_{bz} = \dot{z}_1 + (x_1 - l_u\beta_p)\dot{\beta}_T + y_1\sin(\beta_p + \beta_T) \tag{13}$$

$$V_{fz} = \dot{z}_F + x\dot{\alpha}_s\cos\psi - x\dot{\psi}_s\sin\psi + x_{cg}\dot{\alpha}_s - y_{cg}\dot{\phi}_s \tag{14}$$

**Blade Airloads**

The blade aerodynamic sectional loads are calculated using the local velocity components parallel and perpendicular to the blade reference axis. The incident velocity at a particular blade station consists of three components: the airframe velocity, the blade velocity, and the velocity induced by fuselage motion.

The teetering-motion-induced blade velocity (at point $P_{\eta_r}$ at three-quarter chord on the rotating deformed blade) is given by

$$U_R/\Omega R = -w\dot{\beta}_T - \eta_r\sin\theta_0\dot{\beta}_T + w'x\dot{\beta}_T + \lambda\beta_T + \mu w'\beta_T\cos\psi + \mu\beta_p\beta_T\cos\psi + l_u\dot{\beta}_T \tag{15}$$

$$U_T/\Omega R = \cos\theta_0(-w\beta_T - x\beta_p\beta_T + l_u\beta_T + x\dot{\beta}_T\hat{\phi} + \mu\beta_T\hat{\phi}\cos\psi) + \sin\theta_0(x\dot{\beta}_T + v\beta_T + \mu\beta_T\cos\psi) \tag{16}$$

$$U_P/\Omega R = \sin\theta_0(-w\beta_T - x\beta_p\beta_T + l_u\beta_T + x\dot{\beta}_T\hat{\phi} + \mu\beta_T\hat{\phi}\cos\psi) + \cos\theta_0(x\dot{\beta}_T + v\beta_T + \mu\beta_T\cos\psi) + \eta_r\beta_T \tag{17}$$

The velocity components at a blade section in the blade deformed frame due to hub motion are

$$U_{R_f}\big/\Omega R = (\dot{x}_F - h\dot{\alpha}_s - y_{cg}\dot{\psi}_s)\cos\psi + (\dot{y}_F + \dot{\psi}_s h + x_{cg}\dot{\psi}_s)\sin\psi \tag{18}$$

$$U_{T_f}\big/\Omega R = \cos\theta_0[(\dot{x}_F - h\dot{\alpha}_s - y_{cg}\dot{\psi}_s)\sin\psi + (\dot{y}_F + h\dot{\phi}_s + x_{cg}\dot{\psi}_s)\cos\psi + x\dot{\psi}_s] + \sin\theta_0(\dot{z}_F - x\dot{\phi}_s\sin\psi + x\dot{\alpha}_s\cos\psi + x_{cg}\dot{\alpha}_s - y_{cg}\dot{\phi}_s) \tag{19}$$

$$U_{P_f}\big/\Omega R = \sin\theta_0[(\dot{x}_F - h\dot{\alpha}_s + y_{cg}\dot{\psi}_s)\sin\psi - (\dot{y}_F + h\dot{\phi} + x_{cg}\dot{\psi}_s)\cos\psi - x\dot{\psi}_s] + \cos\theta_0(\dot{z}_F - x\dot{\phi}_s\sin\psi + x\dot{\alpha}_s\cos\psi + x_{cg}\dot{\alpha}_s - y_{cg}\dot{\phi}_s) \tag{20}$$

**Hub Loads**

The hub loads are calculated using a force summation method. For this, the motion-induced aerodynamic and inertial loads are integrated over the blade span to obtain blade loads at the root and then summed over the blades to obtain the rotor hub loads. The resultant blade section inertial loads induced by teetering and fuselage motions are

$$L_u^I = -m[(w + e_g\sin\theta_0)\beta_T + l_u(\ddot{\beta}_T - \beta_T) - 2(\dot{w} + \dot{\theta}_0 e_g\cos\theta_0)\dot{\beta}_T + \ddot{x}_F\cos\psi + \ddot{y}_F\sin\psi - h\ddot{\alpha}_s\cos\psi + h\ddot{\phi}_s\sin\psi - 2x\dot{\psi}_s + (x_{cg}\sin\psi - y_{cg}\cos\psi)\ddot{\psi}_s] \tag{21}$$

$$L_v^I = -m[-2(w + e_g\sin\theta_0)\dot{\beta}_T - 2x\dot{\beta}_T(\beta_p + \beta_T) - 2\beta_T\dot{w} + 2l_u\dot{\beta}_T - \ddot{x}_F\sin\psi + \ddot{y}_F\cos\psi + h\ddot{\alpha}_s\sin\psi + h\ddot{\phi}_s\cos\psi + (x + x_{cg}\cos\psi + y_{cg}\sin\psi)\ddot{\psi}_s] \tag{22}$$

$$L_w^I = -m[x\ddot{\beta}_T + x\beta_T + 2\beta_T\dot{v} - 2\beta_T\dot{\theta}_0 e_g\sin\theta_0 + \ddot{z}_F + (x\cos\psi + x_{cg})\ddot{\alpha}_s - 2x\dot{\alpha}_s\sin\psi - (x\sin\psi + y_{cg})\ddot{\phi}_s - 2x\dot{\phi}_s\cos\psi] \tag{23}$$

$$M_u^I = -m[x\beta_T e_g\cos\theta_0] \tag{24}$$

Terms up to second order are retained in the preceding equations in accordance with the ordering scheme. Thus, the resultant blade section inertial moments induced by fuselage motions are neglected because they are higher-order terms.

**Fuselage Model**

An elastic line airframe structural modeling capability is incorporated into UMARC. The fuselage is discretized as an elastic beam using the same 15-degree-of-freedom beam element as that used for the rotor blade. The elastic line model of the AH-1G helicopter is shown in Fig. 2. In modeling the main fuselage, tailboom, wing, and main rotor shaft, 39 beam elements are used. A spring element is used to model the main rotor pylon. The main rotor pylon provides the structural tie between the main rotor and the fuselage. It is attached to the fuselage through the elastomeric mounts and a lift link. The lift link is the primary vertical load path and is very stiff in the vertical direction. The elastomeric mounts are designed to produce low pylon rocking frequencies to isolate the main rotor in-plane vibratory loads from the fuselage. The pilot seat is located

**Table 1 AH-1G elastic line airframe model**

| Mode | Natural frequency, Hz (/rev) | | |
|---|---|---|---|
| | Present | NASTRAN | Test |
| M/R pylon pitch | 2.75 (0.51) | 3.02 (0.56) | 3.90 (0.72) |
| M/R pylon roll | 3.84 (0.71) | 4.24 (0.79) | —— |
| First fuselage lateral bending | 7.02 (1.30) | 6.80 (1.26) | 7.10 (1.31) |
| First fuselage vertical bending | 7.45 (1.38) | 7.93 (1.47) | 8.00 (1.48) |
| Second fuselage lateral bending | 16.53 (3.06) | 16.70 (3.09) | 18.90 (3.50) |
| Second fuselage vertical bending | 16.80 (3.11) | 17.86 (3.31) | 18.00 (3.33) |
| M/R mast lateral bending | 24.68 (4.57) | 24.79 (4.59) | —— |
| M/R mast F/A bending | 26.41 (4.89) | 25.80 (4.78) | —— |
| Third fuselage vertical bending | 27.54 (5.10) | 29.47 (5.46) | —— |

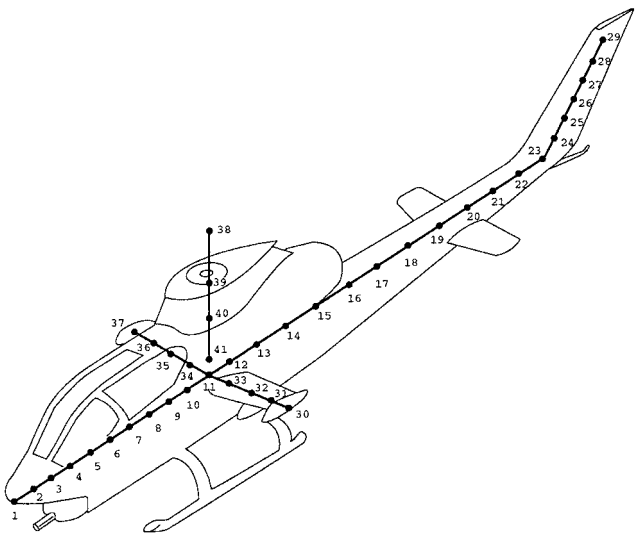

**Fig. 2 Elastic line fuselage model.**

at node 7. Calculated airframe natural frequencies from the present model are compared with NASTRAN predictions and test data in Table 1.

#### Coupled Rotor/Fuselage Equations

Blade response equations are expressed as

$$\boldsymbol{M}_b\ddot{\boldsymbol{q}}_b + \boldsymbol{C}_b\dot{\boldsymbol{q}}_b + \boldsymbol{K}_b\boldsymbol{q}_b + \boldsymbol{M}_{bt}\ddot{\beta}_T + \boldsymbol{C}_{bt}\dot{\beta}_T + \boldsymbol{K}_{bt}\beta_T + \boldsymbol{M}_{bf}\ddot{\boldsymbol{q}}_f + \boldsymbol{C}_{bf}\dot{\boldsymbol{q}}_f + \boldsymbol{K}_{bf}\boldsymbol{q}_f = \boldsymbol{F}_b \tag{25}$$

where $\boldsymbol{q}_b$ is the blade global displacement vector, $\beta_T$ is the teeter angle, $\boldsymbol{q}_f$ is the fuselage displacement vector, and $\boldsymbol{M}_{bf}$, $\boldsymbol{C}_{bf}$, and $\boldsymbol{K}_{bf}$ express the influences of the fuselage motion on the blade response.

Fuselage response equations are given by

$$\left(\boldsymbol{M}_{F1}\ddot{\boldsymbol{q}}_1 + \cdots + \boldsymbol{M}_{FN_b}\ddot{\boldsymbol{q}}_{N_b}\right) + \left(\boldsymbol{C}_{F1}\dot{\boldsymbol{q}}_1 + \cdots + \boldsymbol{C}_{FN_b}\dot{\boldsymbol{q}}_{N_b}\right) + \left(\boldsymbol{K}_{F1}\boldsymbol{q}_1 + \cdots + \boldsymbol{K}_{FN_b}\boldsymbol{q}_{N_b}\right) + \boldsymbol{M}_{Ft_1}\ddot{\beta}_{T_1} + \boldsymbol{C}_{Ft_1}\dot{\beta}_{T_1} + \boldsymbol{K}_{Ft_1}\beta_{T_1} + \boldsymbol{M}_{Ft_2}\ddot{\beta}_{T_2} + \boldsymbol{C}_{Ft_2}\dot{\beta}_{T_2} + \boldsymbol{K}_{Ft_2}\beta_{T_2} + \boldsymbol{M}_f\ddot{\boldsymbol{q}}_f + \boldsymbol{C}_f\dot{\boldsymbol{q}}_f + \boldsymbol{K}_f\boldsymbol{q}_f = \boldsymbol{F}_f \tag{26}$$

where $\boldsymbol{q}_{b1}, \ldots, \boldsymbol{q}_{bN_b}$ are global displacements of each blade.

The equations of motion for the teeter degree of freedom of a two-bladed rotor are obtained from the equilibrium of flap moment about the teeter hinge. The teeter moment $M_T$ is the root flapwise bending moment from the two blades:

$$M_T = \sum_{m=1}^{2}(-1)^m M_y^m \tag{27}$$

Without damper and spring constraints about the teeter hinge, the equations of motion can be obtained from the following equation:

$$M_{t_2}\ddot{\beta}_{T_2} + C_{t_2}\dot{\beta}_{T_2} + K_{t_2}\beta_{T_2} + \boldsymbol{M}_{tb_2}\ddot{\boldsymbol{q}}_{b_2} + \boldsymbol{C}_{tb_2}\dot{\boldsymbol{q}}_{b_2} + \boldsymbol{K}_{tb_2}\boldsymbol{q}_{b_2} + \boldsymbol{M}_{tf_2}\ddot{\boldsymbol{q}}_{f_2} + \boldsymbol{C}_{tf_2}\dot{\boldsymbol{q}}_{f_2} + \boldsymbol{K}_{tf_2}\boldsymbol{q}_{f_2} - M_{t_1}\ddot{\beta}_{T_1} - C_{t_1}\dot{\beta}_{T_1} - K_{t_1}\beta_{T_1} - \boldsymbol{M}_{tb_1}\ddot{\boldsymbol{q}}_{b_1} - \boldsymbol{C}_{tb_1}\dot{\boldsymbol{q}}_{b_1} - \boldsymbol{K}_{tb_1}\boldsymbol{q}_{b_1} - \boldsymbol{M}_{tf_1}\ddot{\boldsymbol{q}}_{f_1} - \boldsymbol{C}_{tf_1}\dot{\boldsymbol{q}}_{f_1} - \boldsymbol{K}_{tf_1}\boldsymbol{q}_{f_1} = f_{t2} - f_{t1} \tag{28}$$

To reduce computational time, the finite element equations are transformed into the normal mode space. To calculate the natural frequencies and mode shapes, the external loads and damping matrix are neglected:

$$\boldsymbol{M}_b^s\ddot{\boldsymbol{q}}_b + \boldsymbol{K}_b^s\boldsymbol{q}_b = 0 \Rightarrow \boldsymbol{q}_b = \boldsymbol{\Phi}_b\boldsymbol{p}_b \tag{29}$$

$$\boldsymbol{M}_f^s\ddot{\boldsymbol{q}}_f + \boldsymbol{K}_f^s\boldsymbol{q}_f = 0 \Rightarrow \boldsymbol{q}_f = \boldsymbol{\Phi}_f\boldsymbol{p}_f = \boldsymbol{\Phi}_{\mathrm{f_e}}\boldsymbol{p}_{\mathrm{f_e}} + \boldsymbol{\Phi}_{\mathrm{f_r}}\boldsymbol{p}_{\mathrm{f_r}} \tag{30}$$

where $\boldsymbol{\Phi}_{\mathrm{f_e}}$ are fuselage elastic mode shapes and $\boldsymbol{\Phi}_{\mathrm{f_r}}$ are fuselage rigid mode shapes.

Blade response equations, teetering motion equations, and fuselage response equations are solved simultaneously. Multiblade coordinate transformation is used to obtain the coning and teetering modes. To avoid singularity of the system, fuselage rigid-body motion terms are moved to the right-hand side of the equations. The final equations are as follows:

$$\begin{bmatrix} \boldsymbol{M}_{rr} & \boldsymbol{M}_{rt} & \boldsymbol{M}_{r\mathrm{f_e}} \\ \boldsymbol{M}_{tr} & M_{tt} & \boldsymbol{M}_{t\mathrm{f_e}} \\ \boldsymbol{M}_{fr} & \boldsymbol{M}_{ft} & \boldsymbol{M}_{f\mathrm{f_e}} \end{bmatrix} \begin{Bmatrix} \ddot{\boldsymbol{\xi}} \\ \ddot{\beta}_G \\ \ddot{\boldsymbol{p}}_{\mathrm{f_e}} \end{Bmatrix} + \begin{bmatrix} \boldsymbol{C}_{rr} & \boldsymbol{C}_{rt} & \boldsymbol{C}_{r\mathrm{f_e}} \\ \boldsymbol{C}_{tr} & C_{tt} & \boldsymbol{C}_{t\mathrm{f_e}} \\ \boldsymbol{C}_{fr} & \boldsymbol{C}_{ft} & \boldsymbol{C}_{f\mathrm{f_e}} \end{bmatrix} \begin{Bmatrix} \dot{\boldsymbol{\xi}} \\ \dot{\beta}_G \\ \dot{\boldsymbol{p}}_{\mathrm{f_e}} \end{Bmatrix} + \begin{bmatrix} \boldsymbol{K}_{rr} & \boldsymbol{K}_{rt} & \boldsymbol{K}_{r\mathrm{f_e}} \\ \boldsymbol{K}_{tr} & K_{tt} & \boldsymbol{K}_{t\mathrm{f_e}} \\ \boldsymbol{K}_{fr} & \boldsymbol{K}_{ft} & \boldsymbol{K}_{f\mathrm{f_e}} \end{bmatrix} \begin{Bmatrix} \boldsymbol{\xi} \\ \beta_G \\ \boldsymbol{p}_{\mathrm{f_e}} \end{Bmatrix} = \begin{Bmatrix} \boldsymbol{F}_{rr} - \boldsymbol{M}_{r\mathrm{f_r}}\ddot{\boldsymbol{p}}_{\mathrm{f_r}} - \boldsymbol{C}_{r\mathrm{f_r}}\dot{\boldsymbol{p}}_{\mathrm{f_r}} \\ F_{tt} - \boldsymbol{M}_{t\mathrm{f_r}}\ddot{\boldsymbol{p}}_{\mathrm{f_r}} - \boldsymbol{C}_{t\mathrm{f_r}}\dot{\boldsymbol{p}}_{\mathrm{f_r}} \\ \boldsymbol{F}_{f\mathrm{f_e}} - \boldsymbol{C}_{f\mathrm{f_r}}\dot{\boldsymbol{p}}_{\mathrm{f_r}} \end{Bmatrix} \tag{31}$$

where subscripts $r$, $t$, and $f$ refer to rotor, teetering motion, and fuselage, respectively, and $\beta_G = \beta_{T_{(m)}}(-1)^m$ for the $m$th blade.

The coupled rotor/fuselage equations are nonlinear, periodic, ordinary differential equations. A temporal finite element method is used to discretize the temporal dependence of the rotor/fuselage equations. Both blade and fuselage displacements are transformed to the temporal nodal displacements using temporal shape functions. Because periodic blade forces are transmitted to the fuselage, the response of the fuselage is also periodic. Therefore, periodic boundary conditions are applied to the fuselage response as well as the blade response. A coupled trim procedure is carried out to solve the blade response, fuselage elastic response, fuselage rigid response, pilot control setting, and vehicle orientation simultaneously.

In this analysis, the couplings between rotor and fuselage are achieved at the hub, and the equilibrium of both steady and vibratory hub loads are satisfied. Aerodynamic loads acting on the fuselage are not considered.

## Results and Discussion

The two-bladed teetering rotor of the AH-1G helicopter is used in this analysis. The description of the baseline configuration is given in Table 2. Coupled rotor/fuselage equations are solved in straight and level flight conditions. Then vibration results calculated by the present analysis are compared with OLS flight test data.[11]

The blade is discretized into 13 beam elements with each element consisting of 15 degrees of freedom and the blade mass and stiffness distributions are given in Table 3. Its collective mode (cantilevered boundary condition) natural frequencies are given in Table 4 (see Ref. 19) and compared with those used by the C81 program (a comprehensive rotor analysis developed by Bell Helicopter).[20,21] DNAM06 was used to compute coupled rotor natural frequencies and mode shapes using Myklestad rotating beam analysis and to

**Table 2 Blade properties**

| Property | Value |
|---|---|
| Number of blade | 2 |
| Rotor radius | 22 ft |
| Chord | 27 in. |
| Rotor speed | 324 rpm |
| Lock number | 5.078 |
| Precone angle | 2.75 deg |
| Twist at tip | −10 deg |
| Control system spring rate | 396,000 in.-lb/rad |
| Pitch link moment arm | 9.067 in |
| Pitch horn attachment radial station | 14.1 in. |
| Lift curve slope | 6.159 |
| Flapping inertia $I_\beta$ | 1,499.704 slug-ft$^2$/blade |
| Mass/blade | 504.298 lbf |
| Rotor pitch/flap coupling $\delta_3$ | 0 deg |
| Undersling | 4.5 in. |

**Table 3 Blade mass and stiffness distribution**

| Element number | Length | Mass | $EI_z$ | $EI_y$ | GJ |
|---|---|---|---|---|---|
| 1 | 0.013258 | 7.31640 | 0.304930 | 0.0210210 | 0.0021940 |
| 2 | 0.028410 | 2.26044 | 0.254970 | 0.0005264 | 0.0021940 |
| 3 | 0.011740 | 6.37690 | 0.517574 | 0.0207530 | 0.0021940 |
| 4 | 0.088640 | 5.63326 | 0.103860 | 0.0181830 | 0.0021220 |
| 5 | 0.013258 | 6.32570 | 0.027462 | 0.0487600 | 0.0040840 |
| 6 | 0.044700 | 3.64410 | 0.501722 | 0.0248600 | 0.0051562 |
| 7 | 0.108710 | 0.75620 | 0.252660 | 0.0045400 | 0.0041053 |
| 8 | 0.191290 | 0.73440 | 0.248113 | 0.0030600 | 0.0028160 |
| 9 | 0.090150 | 0.69964 | 0.213710 | 0.0024400 | 0.0020840 |
| 10 | 0.109850 | 0.95505 | 0.188814 | 0.0024900 | 0.0020600 |
| 11 | 0.104170 | 1.01890 | 0.161512 | 0.0024100 | 0.0020600 |
| 12 | 0.097730 | 1.08473 | 0.161673 | 0.0025700 | 0.0020600 |
| 13 | 0.098110 | 1.03680 | 0.163053 | 0.0024500 | 0.0020600 |

**Table 4 Blade natural frequencies**

| Mode | Present (/rev) | C81 input (/rev)[19] |
|---|---|---|
| Flap 1 | 1.04 | 1.04 |
| Flap 2 | 2.85 | 3.01 |
| Flap 3 | 4.76 | 4.68 |
| Lag (rigid pylon) | 1.45 | —— |
| Lag (flexible pylon) | 1.65 | 1.60 |
| Torsion | 2.47 | 2.27 |

provide input data to the C81 code. Two lag frequencies are used in the present analysis. The OLS rotor has a relatively flexible pylon in the in-plane direction, and the pylon flexibility has an influence on the in-plane frequency. First, it is assumed to be an infinitely rigid pylon along with the hub-fixed model and elastic fuselage model. Second, a coupled rotor/flexible pylon model is used. This increases the first coupled lag mode frequency by about 14%. DNAM06 also used in-plane pylon impedance to consider the flexibility of the pylon. The corresponding predicted blade frequencies from the two different analyses agree well with each other (deviation less than 3%).

A comparison of calculated rotor trim control angles with flight-test data is shown in Fig. 3. The collective angle agrees well with test data at low speeds and underpredicts slightly at high speeds. The analysis underpredicts both longitudinal and lateral cyclic angles by up to 3 deg.

Blade chord bending moment, beam bending moment, and torsional moment are presented in Figs. 4–9 as a function of blade radius position at low and high speeds and are compared with flight-test data. Three different analysis options are used for each case. The first is the hub-fixed model, the second is the elastic line model with rigid pylon, and the third is the full elastic line body model with flexible shaft and pylon. The first case represents the hub-fixed condition, and the rotor/fuselage coupling effect is neglected.

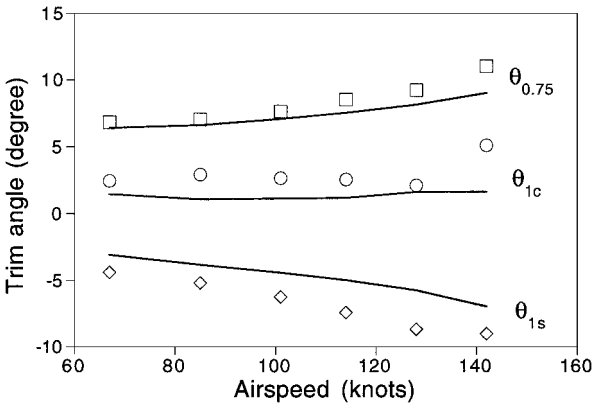


**Fig. 3 Rotor control angles.**

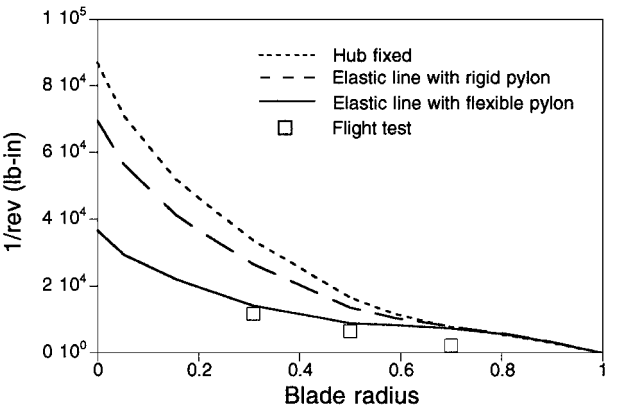


**1/rev component**

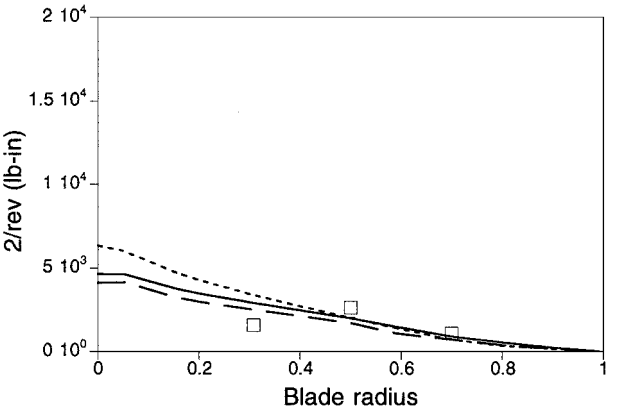


**2/rev component**

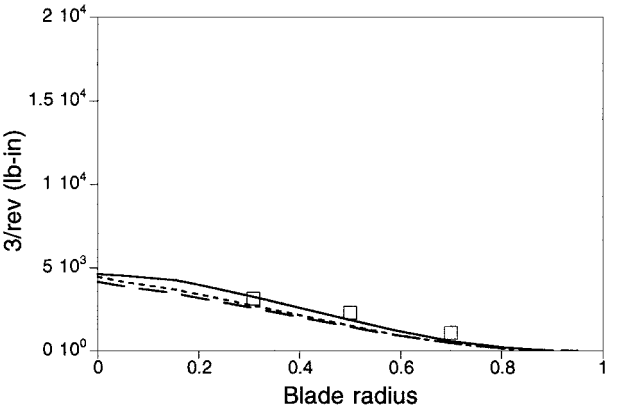


**3/rev component**

**Fig. 4 Blade chord bending moments at 67 kn.**

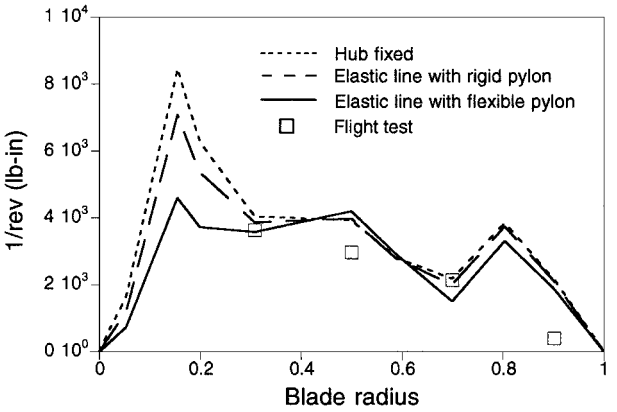


1/rev component

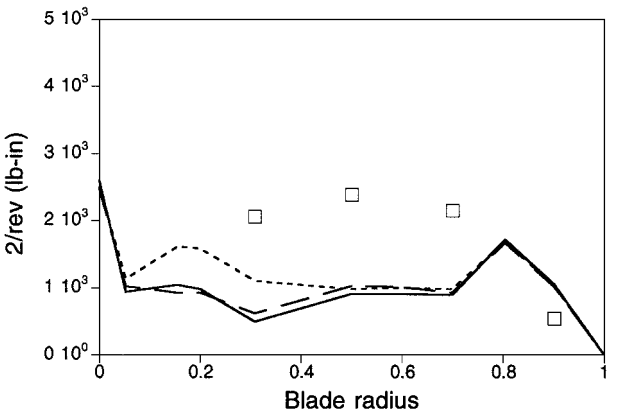


2/rev component

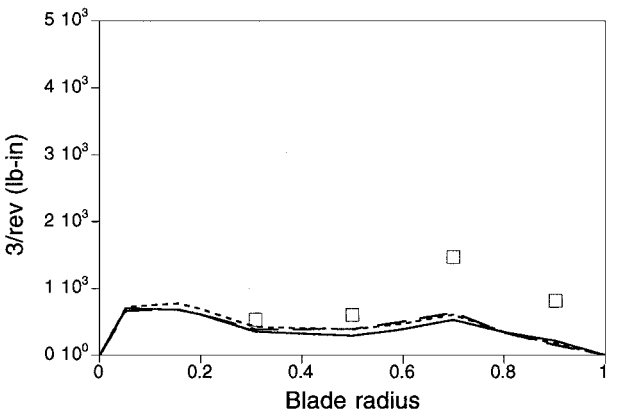


3/rev component

**Fig. 5 Blade beam bending moments at 67 kn.**

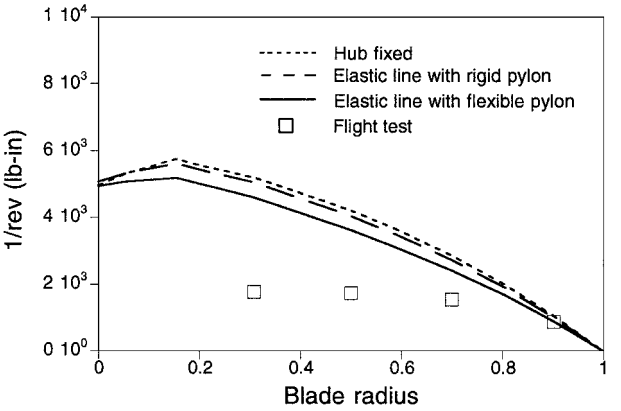


1/rev component

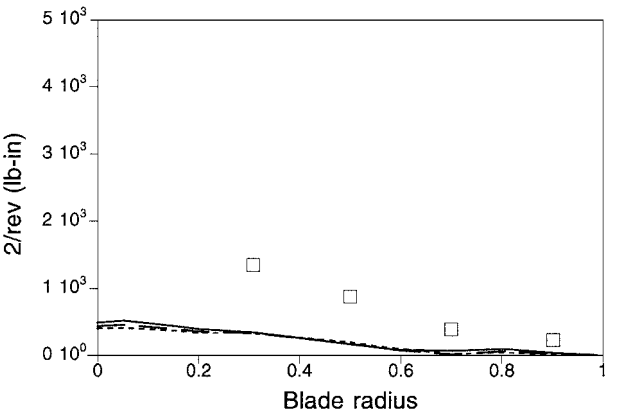


2/rev component

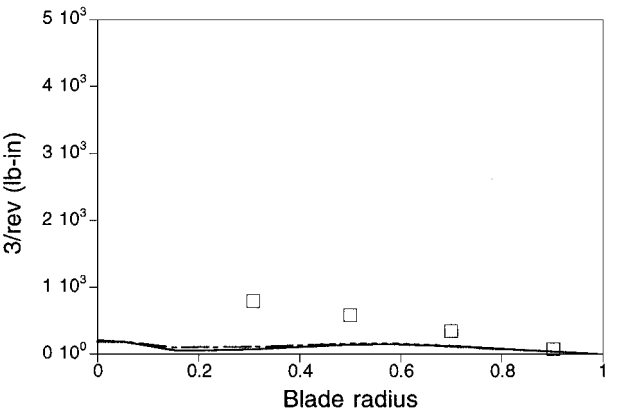


3/rev component

**Fig. 6 Blade torsional moments at 67 kn.**

For the second case, the rotor shaft is assumed to be rigidly attached to the fuselage. Therefore, the three translational (axial, vertical, and lateral) and three rotational (pitch, roll, and yaw) fuselage motions at the node adjacent to the shaft have a direct effect on the blade dynamics. For the third case, main rotor pylon and shaft bending motion as well as elastic fuselage motions are included to determine blade loads.

At the speed of 67 kn ($\mu = 0.15$), estimated chord bending moments show good agreement with test data (Fig. 4). When the rotor/fuselage coupling is neglected, the 1/rev component is dramatically overpredicted. The elastic line model with a rigid pylon reduces 1/rev root bending moment by about 20% but has a small effect on the other harmonic components. Pylon flexibility reduces especially 1/rev harmonic component along the blade span and improves the correlation between the analysis and flight-test data. Pylon flexibility increases lag frequency above 1/rev; hence, the 1/rev chord bending moment is reduced. Calculated beam bending moments show the same trend as the test data (Fig. 5). Figure 5 shows that a teetering rotor has both articulated and hingeless rotor characteristics. The zero root moment of 1/rev and 3/rev components shows the characteristics of an articulated rotor without hinge offset, and a nonzero root moment for the 2/rev component shows the characteristics of a hingeless rotor. The correlation of this moment is not as good as that of chord bending moment. Calculated torsional moments overpredict 1/rev harmonic and underpredict 2/rev and 3/rev harmonics (Fig. 6). The rotor/fuselage coupling effect is small in the torsional moment.

Figures 7–9 show results for blade vibratory moment distribution for a forward speed of 142 kn ($\mu = 0.32$). Again, the pylon flexibility has a significant influence on the chordwise bending moment.

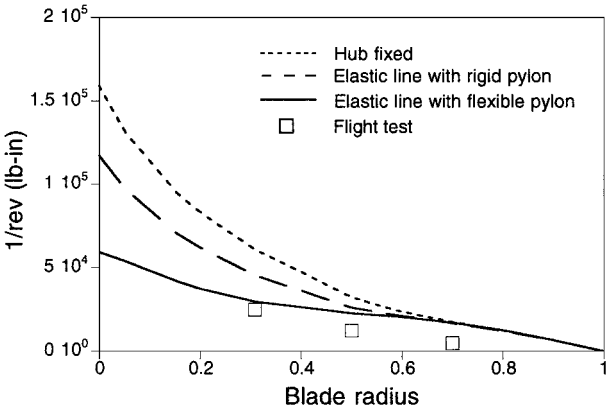


1/rev component

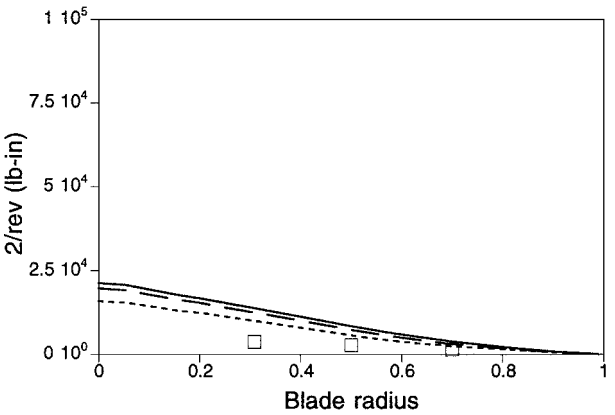


2/rev component

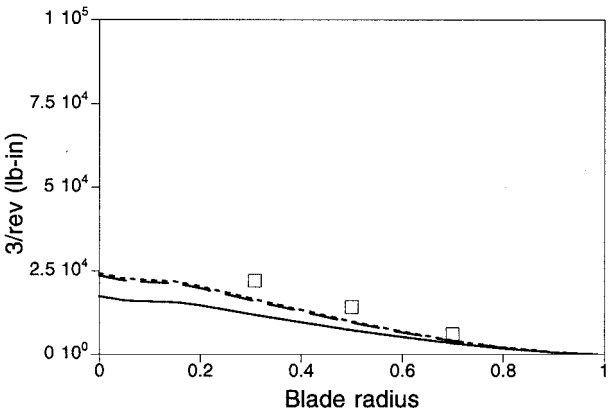


3/rev component

**Fig. 7 Blade chord bending moments at 142 kn.**

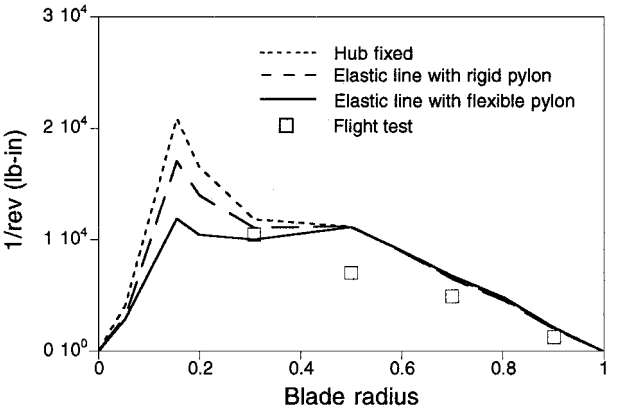


1/rev component

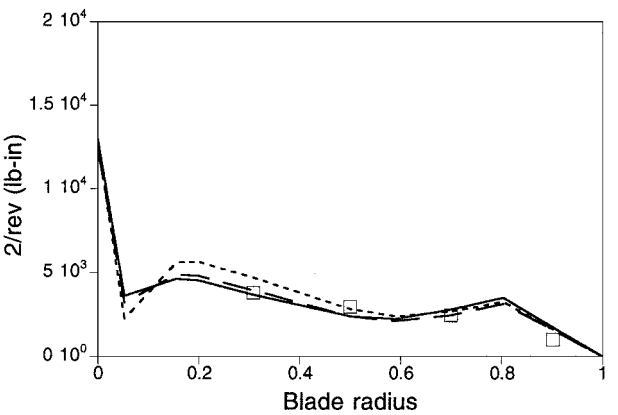


2/rev component

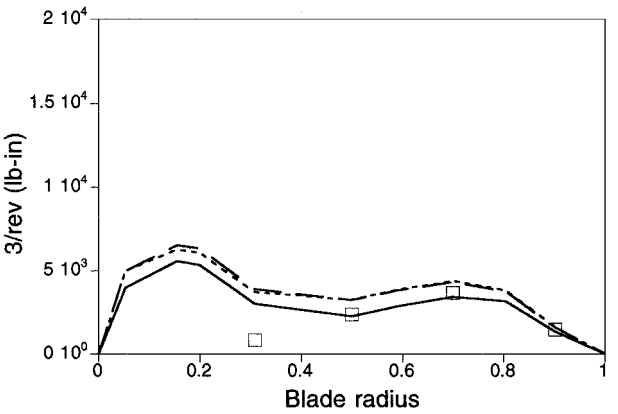


3/rev component

**Fig. 8 Blade beam bending moments at 142 kn.**

The elastic line model reduces the 1/rev chord bending moment along the blade, thus significantly improving the correlation with flight-test data. Estimation of beam bending moments at this speed show better correlation than that at low speed. The 2/rev component shows especially good correlation with test data. As compared to the earlier case at low speed, the 1/rev torsional moment component is increased to almost twice for both prediction and flight-test values. Again, the comparison of the 1/rev component shows the same difference as that at low speed. The 2/rev component shows better correlation than low speed. Prediction of the 3/rev component is well matched with flight-test data.

Figures 10 and 11 show 2/rev and 4/rev hub forces. Flight-test data are not available for these forces; hence, predicted vibratory hub forces are compared with those predicted using the C81 analysis combined with a three-dimensional NASTRAN fuselage model.[22]

The C81 analysis has incorporated two trim strategies.[23] The first trim solution is called trim to cyclic and is similar to a wind-tunnel trim solution where measured blade feathering and aircraft attitudes are input to the C81 code. This technique can be used only when test data are available. The second trim solution is called full aircraft trim and uses only flight conditions as inputs to C81, and then C81 calculates all of the control positions required to trim the helicopter. The trim procedure of the present analysis is basically the same as full aircraft trim in the C81 program.

Rotor/fuselage coupling reduces 2/rev longitudinal and lateral hub forces and has negligible effect on 2/rev vertical hub force and all three 4/rev hub forces. Rotor/fuselage coupling due to pylon flexibility has a dramatic effect on the prediction of 2/rev longitudinal and lateral hub forces. Both the present analysis and the C81 analysis predict similar 2/rev lateral and vertical hub forces.

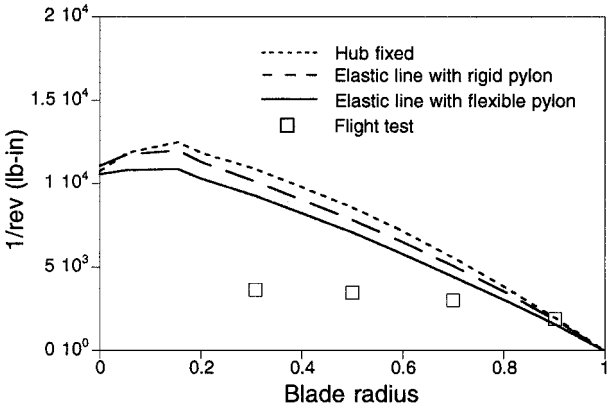


1/rev component

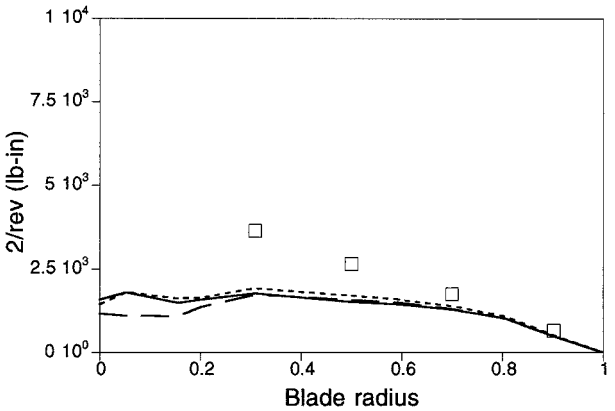


2/rev component

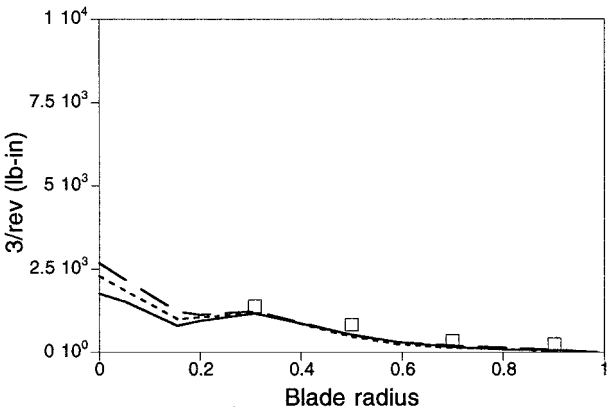


3/rev component

**Fig. 9 Blade torsional moments at 142 kn.**

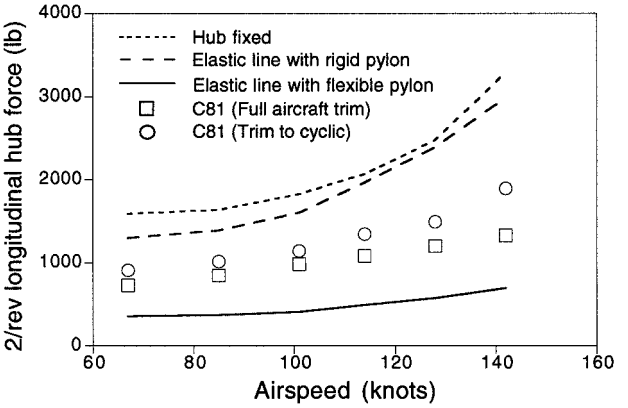


2/rev longitudinal hub force

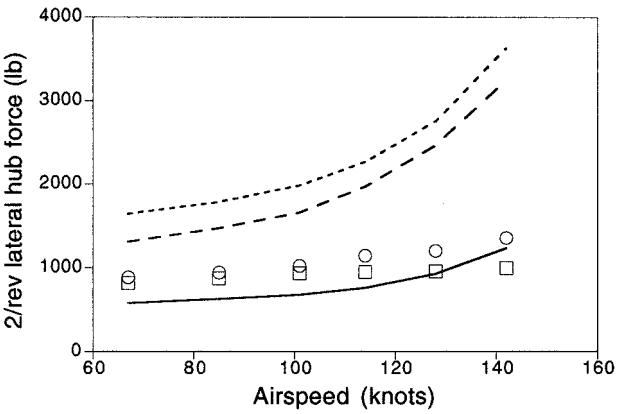


2/rev lateral hub force

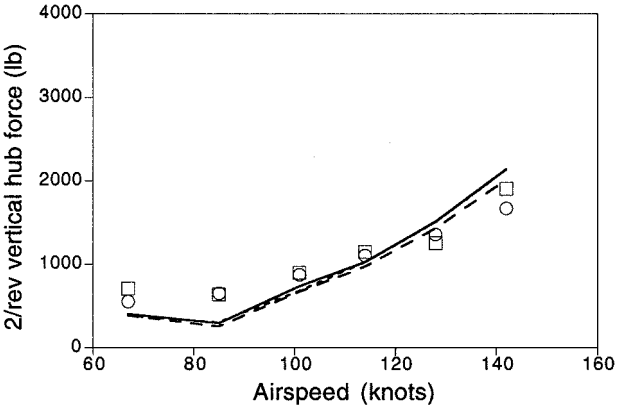


2/rev vertical hub force

**Fig. 10 Hub forces, 2/rev.**

However, the prediction of the present analysis for longitudinal hub force is lower than that of C81.

Vibration levels at the pilot seat are presented in Fig. 12 with airspeeds ranging from 67 to 142 kn. Figures 12a and 12b show 2/rev and 4/rev vertical vibration levels. Pylon flexibility reduces predicted 2/rev vibration by up to 23% and has a small effect on 4/rev vibration. For all speeds, 2/rev and 4/rev vibration levels are underpredicted. Figures 12c and 12d show 2/rev and 4/rev lateral vibration levels. Pylon flexibility decreases the predicted magnitude of 2/rev vibration by 43% at 67 kn and by 50% at 142 kn and significantly improves the correlation with test data. However, large deviation from the test results is found at high speed. Again, pylon flexibility has a small effect on 4/rev vibration.

Figure 13 represents vertical and lateral vibration levels at the pilot seat. Three types of aerodynamic models are used. The first is a linear inflow distribution (Drees model) with quasi-steady aerodynamics, the second is a linear inflow distribution with time-domain unsteady aerodynamics (Leishman–Beddoes),[16] and the third is a detailed free-wake model (Bagai–Leishman)[15] with unsteady aerodynamics. The vibration levels estimated using these three aerodynamic models show an important influence on the prediction of vibration. For the 2/rev vertical vibration, unsteady aerodynamics increases the magnitude by 6% at high speed and free wake increases the magnitude by 20% at low speed and 13% at high speed. For the 4/rev vertical vibration, there are significant differences in magnitude with aerodynamic modeling. The simple inflow model shows low to negligible vibration in all flight conditions. Unsteady aerodynamics has more of an influence at high speed. Free wake has a dramatic effect (almost 10 times increase) at low speed and a significant effect (50% increase) even at high speed. The higher harmonic

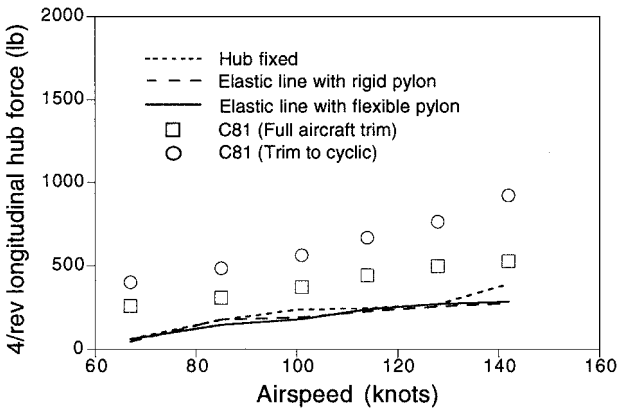


**4/rev longitudinal hub force**

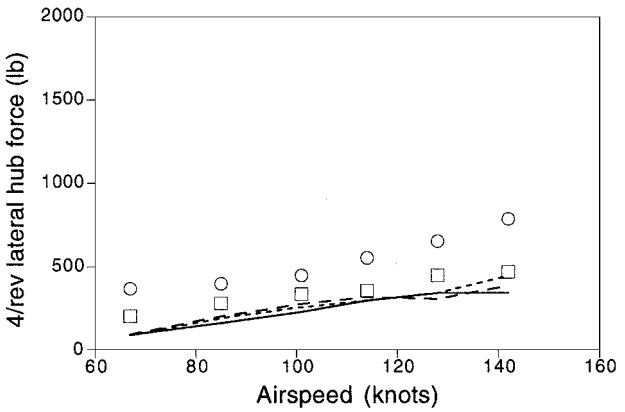


**4/rev lateral hub force**

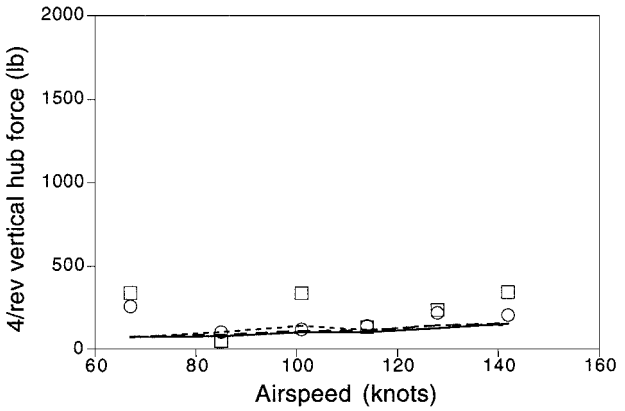


**4/rev vertical hub force**

**Fig. 11 Hub forces, 4/rev.**

airloads come from the rapid variations in velocity perpendicular to the blade due to the vortex wake. The free-wake model captures the higher harmonic vibration by computing the interaction between the blades and the shed and trailed wake, thus significantly improves the correlations with the test data. Results for 2/rev lateral vibration show that the effect of unsteady aerodynamics and free wake on the magnitude is small compared to 2/rev vertical vibration results. For the 4/rev lateral vibration, free wake increases the magnitude at low speed, and unsteady aerodynamics increase the magnitude at high speed.

Figure 14 shows the effect of airframe flexibility on vibration at the pilot seat. Two analysis options are used. First, rotor equations are coupled with fuselage rigid-body motions. Second, both fuselage rigid and elastic motions are coupled with rotor equations. Even though the trend is similar, the differences in magnitude are significant. Rigid fuselage model overpredicts 2/rev vertical and lateral vibrations up to 80 and 130%, respectively.

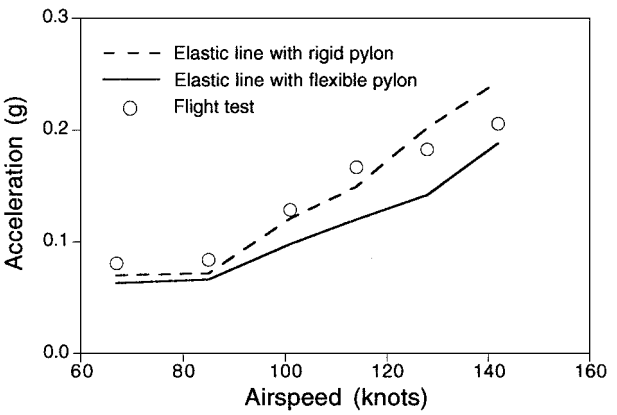


**a) 2/rev vertical vibration**

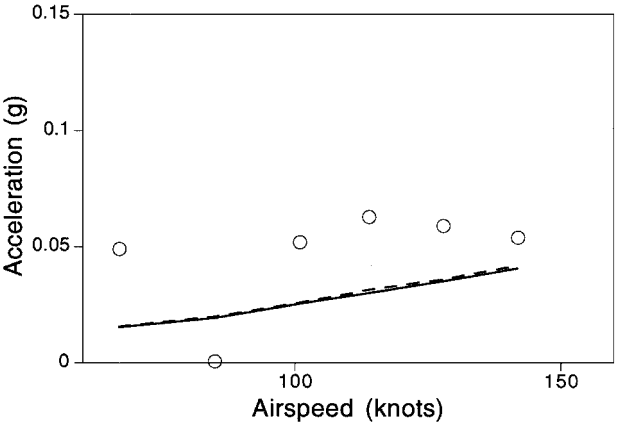


**b) 4/rev vertical vibration**

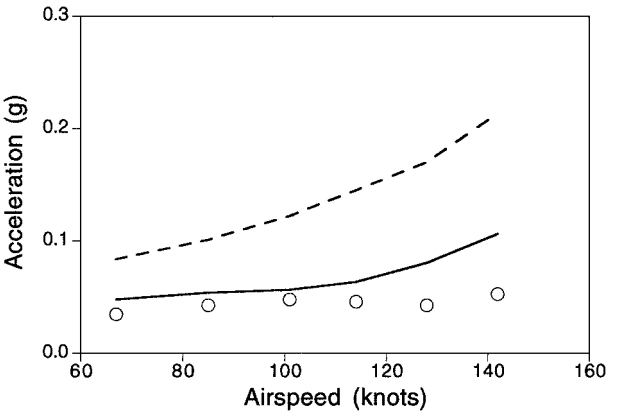


**c) 2/rev lateral vibration**

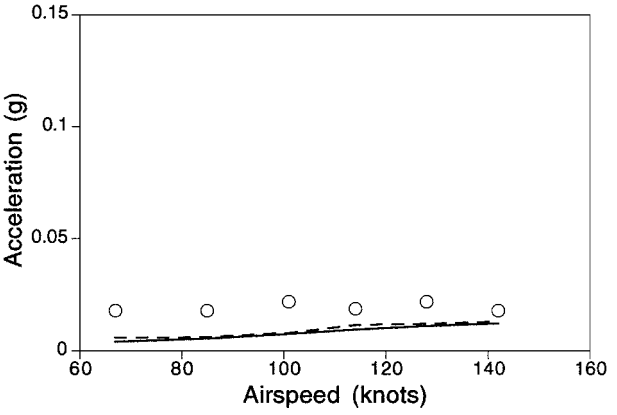


**d) 4/rev lateral vibration**

**Fig. 12 Vibration level at pilot seat.**

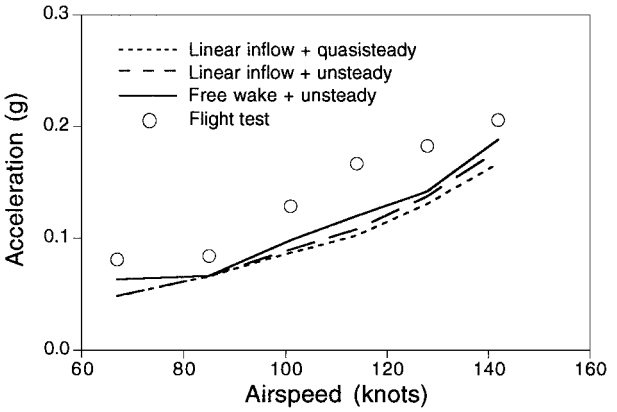


2/rev vertical vibration

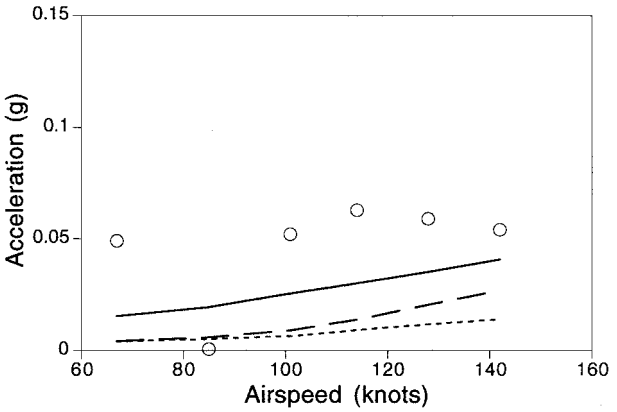


4/rev vertical vibration

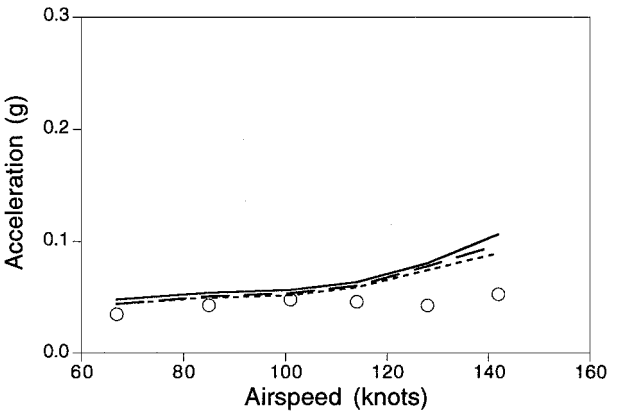


2/rev lateral vibration

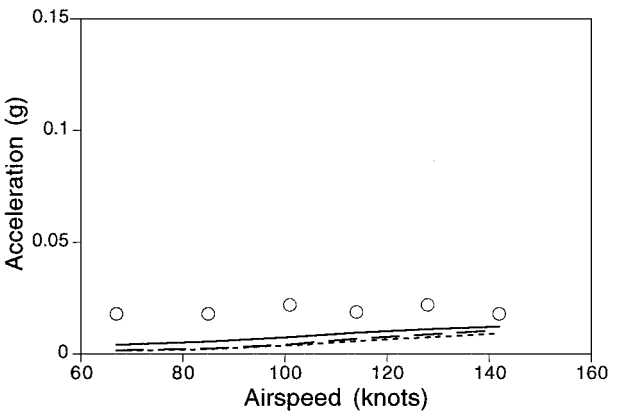


4/rev lateral vibration

**Fig. 13 Effect of aerodynamic model on vibration at pilot seat.**

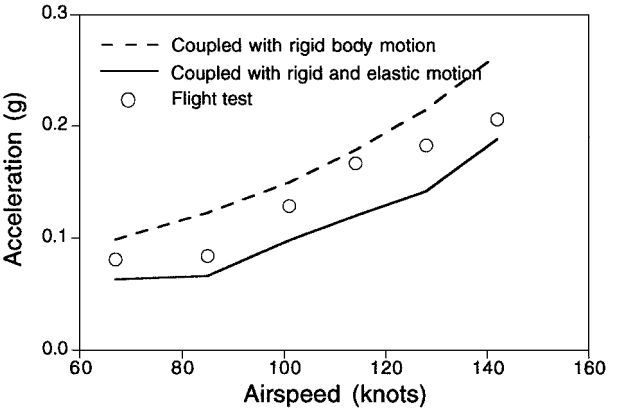


2/rev vertical vibration

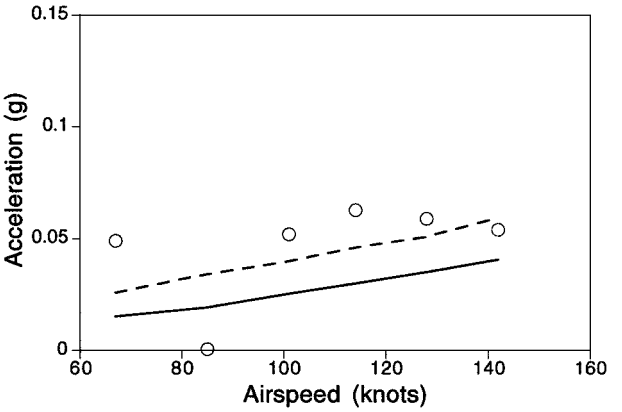


4/rev vertical vibration

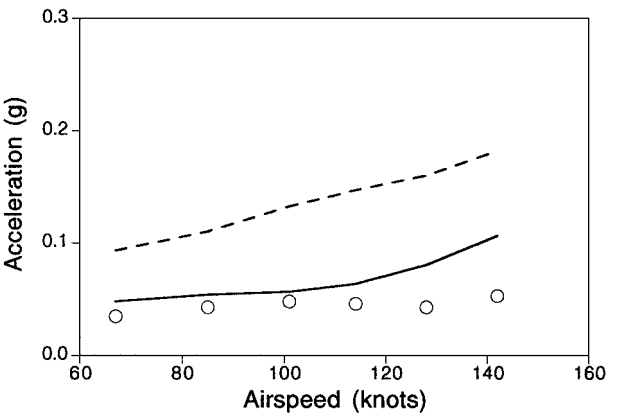


2/rev lateral vibration

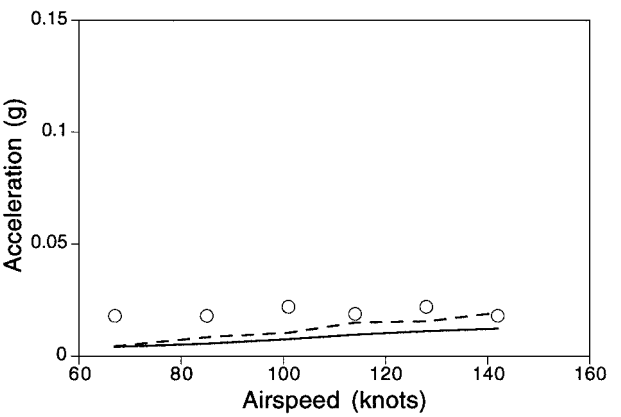


4/rev lateral vibration

**Fig. 14 Effect of airframe flexibility on vibration at pilot seat.**

## Conclusions

A comprehensive vibration analysis of a coupled rotor/fuselage system for a two-bladed teetering rotor using finite element methods in space and time is developed. An elastic fuselage modeling capability is incorporated with an elastic rotor analysis. Effects of pylon and shaft flexibility on the analysis of blade and hub loads and airframe vibration are investigated. Predicted results are evaluated with flight-test data from an AH-1G helicopter. From this study, the following conclusions are drawn:

1) Calculated airframe natural frequencies from the present elastic line model are well matched with NASTRAN predictions.

2) Comparison between calculated blade vibratory chord bending moments and measured data shows fair agreement and the pylon flexibility has a significant effect on the correlation of 1/rev component.

3) Comparison between calculated blade beam bending moments and measured data shows poor to fair agreement both at low and high speeds.

4) Rotor/fuselage coupling and pylon flexibility decrease predicted 2/rev longitudinal and lateral hub forces and have a negligible effect on 4/rev hub forces.

5) The correlation of 2/rev vertical vibration at the pilot seat is generally fair, whereas calculated 4/rev vertical vibration is underpredicted at all speeds.

6) Predicted 2/rev lateral vibration at the pilot seat shows fair correlation with test data up to moderate speeds. At all speeds, 4/rev lateral vibrations are underpredicted.

7) Refined aerodynamics, especially free wake, is essential for the prediction of vibration. For example, free wake increases the magnitude of 4/rev vertical vibration level by 10 times at 67 kn.

## Acknowledgments

This work was supported by the National Rotorcraft Technology Center under Grant NCC 2944, Technical Monitor Yung Yu. The authors thank Raymond Kvaternik (NASA Langley Research Center) and Jing Yen and David Popelka (Bell Helicopter Textron) for providing airframe data and many valuable discussions.

## References

[1]Kvaternik, R. G., Bartlett, F. D., Jr., and Cline, J. H., "A Summary of Recent NASA/Army Contributions to Rotorcraft Vibration and Structural Dynamics Technology," NASA CP-2495, Feb. 1988.

[2]Gerstenberger, W., and Wood, E. R., "Analysis of Helicopter Aeroelastic Characteristics in High-Speed Flight," *AIAA Journal*, Vol. 1, No. 10, 1964, pp. 2366–2381.

[3]Staley, J. A., and Sciarra, J. J., "Coupled Rotor/Airframe Vibration Prediction Methods," *Rotorcraft Dynamics*, NASA SP-352, 1974, pp. 81–90.

[4]Hohenemser, K. H., and Yin, S. K., "The Role of Rotor Impedance in the Vibration Analysis of Rotorcraft," *Vertica*, Vol. 3, Nos. 3, 4, 1979, pp. 187–204.

[5]Hsu, T. K., and Peters, D. A., "Coupled Rotor/Airframe Vibration Analysis by a Combined Harmonic-Balance Impedance Matching Method," 36th Annual Forum of the American Helicopter Society, May 1980.

[6]Gable, R., and Sankewitsch, V., "Rotor–Fuselage Coupling by Impedance," 42nd Annual Forum of the American Helicopter Society, June 1986.

[7]Stephens, W. B., and Peters, D. A., "Rotor-Body Coupling Revisited," *Journal of the American Helicopter Society*, Vol. 32, No. 1, 1987, pp. 68–72.

[8]Vellaichamy, S., and Chopra, I., "Effect of Modeling Techniques in the Coupled Rotor-Body Vibration Analysis," AIAA Paper 93-1360, April 1993.

[9]Chiu, T., and Friedmann, P. P., "A Coupled Helicopter Rotor/Fuselage Aeroelastic Response Model for ACSR," AIAA Paper 95-1226, April 1995.

[10]Hansford, R. E., and Vorwald, J., "Dynamics Workshop on Rotor Vibratory Loads Prediction," *Journal of the American Helicopter Society*, Vol. 43, No. 1, 1998, pp. 76–87.

[11]Dompka, R. V., and Cronkhite, J. D., "Summary of AH-1G Flight Vibration Data for Validation of Coupled Rotor-Fuselage Analysis," NASA CR-178160, Oct. 1987.

[12]DiTaranto, R. A., and Sankewitsch V., "Calculation of Flight Vibration Levels of the AH-1G Helicopter and Correlation with Existing Flight Vibration Measurements," NASA CR-181923, Nov. 1989.

[13]Sangha, K., and Shamie, J., "Correlation of AH-1G Airframe Flight Vibration Data with a Coupled Rotor–Fuselage Analysis," NASA CR-181974, Aug. 1990.

[14]Sopher, R., and Twomey, W. J., "Calculation of Flight Vibration Levels of the AH-1G Helicopter and Correlation with Existing Flight Vibration Measurements," NASA CR-182031, April 1990.

[15]Bagai, A., and Leishman, J. G., "Rotor Free-Wake Modeling Using a Pseudo-implicit Relaxation Algorithm," AIAA Paper 94-1918, June 1994.

[16]Leishman, J. G., "Validation of Approximate Indicial Aerodynamic Functions for Two-Dimensional Subsonic Flow," *Journal of Aircraft*, Vol. 25, No. 10, 1988, pp. 914–922.

[17]*UMARC, University of Maryland Advanced Rotorcraft Code, Theory Manual*, Alfred Gessow Rotorcraft Center, Univ. of Maryland, College Park, MD, July 1994.

[18]Yeo, H., "A Comprehensive Vibration Analysis of a Coupled Rotor/Fuselage System," Ph.D. Dissertation, Dept. of Aerospace Engineering, Univ. of Maryland, College Park, MD, 1999.

[19]Van Gaasbeek, J. R., "Validation of the Rotorcraft Flight Simulation Program (C81) Using Operational Loads Survey Flight Test Data," USAAVRADCOM-TR-80-D-4, July 1980.

[20]McLarty, T. T., "Rotorcraft Flight Simulation Program C81 with Coupled Rotor Aeroelastic Stability Analysis," U.S. Army Air Mobility Research and Development Lab., USAAMRDL TR76-41A, Engineering Manual, May 1977.

[21]Van Gaasbeek, J. R., "Rotorcraft Flight Simulation Program C81 with Datamap Interface," USAAVRADCOM TR-80-D-38A, Users Manual, Oct. 1981.

[22]Cronkhite, J. D., Dompka, R. V., Rogers, J. P., Corrigan, K. C., and Perry, K.S., "Summary of AH-1G OLS Flight Vibration Correlation Analysis Results," NAS1-17496, Oct. 1985.

[23]Dompka, R. V., and Corrigan, J. J., "AH-1G Flight Vibration Correlation Using NASTRAN and the C81 Rotor/Fuselage Coupled Analysis," 42nd Annual Forum of the American Helicopter Society, June 1986.